

High precision LIF measurements of three-dimensional density perturbations

Evgeny Ermanyuk¹, Jan-Bert Flor², Bruno Voisin³

1: Lavrentyev Institute of Hydrodynamics, Novosibirsk, Russia, ermanyuk@hydro.nsc.ru

2: Laboratoire des Ecoulements Geophysiques et Industrielles, Grenoble, France, flor@hmg.inpg.fr

3: Laboratoire des Ecoulements Geophysiques et Industrielles, Grenoble, France, bruno.voisin@legi.grenoble-inp.fr

Abstract This paper reports a novel technique of the 3D measurement of density displacements in a continuously stratified fluid, here applied to internal waves. Iso-density surfaces are marked with thin fluorescein dyed planes and illuminated with a vertical laser sheet. We have developed a technique to obtain highly accurate quantitative data from the displacement of these dye planes. The vertical distribution of luminosity across each plane is cross-correlated with a Gaussian function and subsequently interpolated, allowing for a subpixel resolution of 0.05 pixels. This method combines an appealing visualization with low-noise highly accurate quantitative measurements and has the advantage above the commonly used Schlieren and PIV methods to directly visualize the motion in a plane, to allow for the measurement of vertical velocities with high velocity gradients such as e.g. near obstacles, and gives the possibility to record also lagrangian transports.

Here this method is employed to internal waves. With period-averaged measurements for several vertical equidistant planes, the 3D spatial distribution of internal wave rms amplitudes is reconstructed. As a demonstration we measure the spatial structure of internal waves emitted by a horizontally oscillating sphere in a uniformly stratified fluid.

1. Introduction

There are different techniques to measure internal wave motions in uniformly stratified fluids. Two-dimensional internal-wave fields have been visualized via non-intrusive Schlieren techniques, evolving from its classic form to interferometry and shearing interferometry (Gortler 1943, Mowbray and Rarity 1967, Peters 1985, Merzkirch and Peters 1992, Makarov et al. 1990). Moire fringes have been used in Ivanov (1988, 1989) and Sakai (1990). Although the above-mentioned methods yield high-resolution visualizations of phase patterns, their application requires high-quality optical windows in the test tank walls, with fairly limited field of view. Another disadvantage is related to a difficulty of quantitative measurements of wave field parameters.

The advent of digital image processing has allowed an effective access to quantitative measurements of density-gradient or velocity fields. The synthetic Schlieren technique has been proposed by Sutherland et al. (1999) and Dalziel et al. (2000). It has been applied since then to a number of 2D problems in Sutherland and Linden (2002) Ermanyuk and Gavrilov (2005, 2008), Mercier et al. (2008), Thomas et al. (2009), Clark and Sutherland (2009). The synthetic Schlieren technique is based on automatic processing of optical distortions of a contrast image (say, pattern of black dots or stripes on a white background) observed through a perturbed uniformly stratified fluid. The local apparent distortion of the background image is proportional to the local perturbation of the density gradient. In 3D problems this technique can be used directly for measurements of optical distortions integrated along the light ray path (Peacock and Weidman 2005). A quantitative measurement of axisymmetric internal wave fields, such as for instance those emitted by a vertically oscillating sphere, has been made possible by combining synthetic Schlieren with tomographic inversion (Flynn et al. 2003, Onu et al. 2003). An application to a vertically translating sphere in a uniformly stratified fluid is described in Yick et al. (2010). A theoretical possibility of the tomographic inversion technique for an arbitrary disturbance has been discussed in Decamp et al. (2007) but remains to be applied. An alternative technique of optical tomography is described in Hazewinkel (2010) with application to internal-wave attractors.

Internal waves can also be measured from particle motions using PIV. Accurate PIV

measurements in a continuously stratified fluid require a dense and uniform distribution of particles. However, the preparation of particles matching a given density distribution is often a very elaborative process. Of course, once this problem is resolved, 2D and 3D internal waves fields can be easily measured with the PIV method (Zhang et al. 2007, King et al 2009).

Two decades ago, wave motions were generally visualized by thin dye lines or planes generated at different levels in the fluid, a method that is easy to employ and provides nice images (see e.g. Hopfinger et al. 1991). Quantitative information of such images could be obtained using the distribution of diffused dye of which a Gaussian fit allows for subpixel accuracy. Indeed accurate density measurements were thus obtained in spin-up flows by Flor et al (2002). This idea is here further exploited and refined in an automated processing technique, allowing for the measurement of the 3D spatial structure of internal waves. The accuracy of the method and optimal choice of the governing parameters is discussed. The technique is applied to the measurement of waves emitted by a horizontally oscillating sphere in a uniformly stratified fluid. A geophysical analogue of this problem is represented by the baroclinic tides in the ocean in vicinity of an isolated mountain at the ocean or sea bottom. Important role of baroclinic tides in the energy balance of the ocean (Morozov 1995, Vlasenko et al 2005, Garrett and Kunze 2007) serves as a geophysical motivation for the present experimental study.

2. Experimental setup and data processing

Experiments were carried out in a plexiglas square tank with a working depth of 50 cm and horizontal dimensions of 97×97 cm. The scheme of the experimental setup is shown in Fig. 1a. The tank was filled to a depth of 47 cm with a linearly stratified fluid. Salt was used as stratifying agent and tap water as working fluid. The stratification was measured by taking density samples at different heights in the fluid. The buoyancy frequency $N(z) = [(-g/\rho)(d\rho/dz)]^{1/2}$ in all experiments was kept constant at 1.19 rad/s, where g is the gravity acceleration, $\rho(z)$ is the density distribution over vertical coordinate z . The waves were generated by a horizontally oscillating plexiglass sphere of radius R attached to a pendulum of length 1.3 m. The surface of the sphere was painted black to avoid unwanted laser light reflections. The oscillations of the pendulum were driven by an eccentric wheel. The motion of the sphere was in good approximation horizontal and sinusoidal, with amplitude A and frequency ω . After 10 oscillation periods the wave pattern was stationary. Measurements were taken after 20 oscillations. Images were recorded by 12-bit digital camera DALSA with CCD of 1024×1024 pixels and 8-bit digital camera JAI with CCD of 1388×1030 pixels has been used to check the role played by the bit number. For the imaging area used in the present experiments 1 pixel corresponds to approximately 0.4mm.

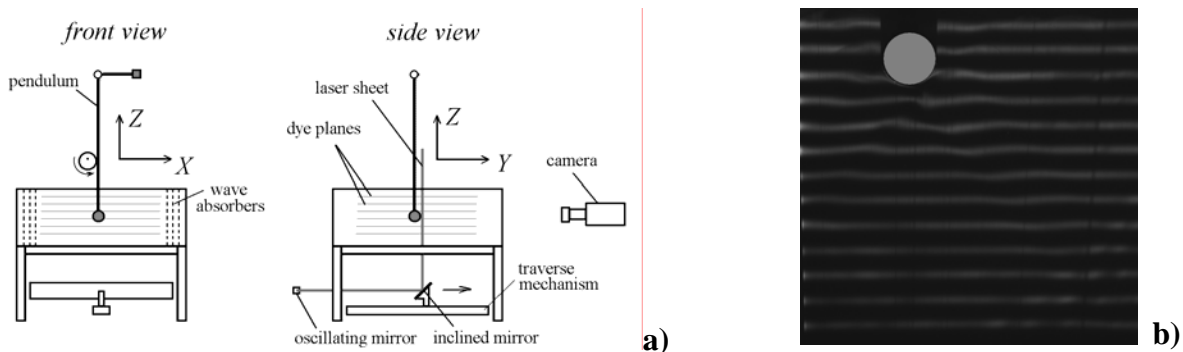


Fig. 1. a) Experimental setup and **b)** typical image of fluorescein lines (oscillating sphere is shown by grey circle)

A set of equidistant horizontal dye planes was generated by carefully displacing a rake of horizontally spanned - and in fluorescein solution soaked - cotton threads through the fluid (see Fig.

2b). The distance between adjacent dye planes was about 2 cm. The dye planes were then illuminated by a vertical laser sheet, passing through the transparent bottom of the tank, and parallel to the plane of oscillation of the sphere. The position of the laser sheet was computer-controlled and changed by moving the inclined mirror on the traverse mechanism (see Fig. 1). To measure period-averaged quantities and determine the amplitudes of Fourier-components of the signal, the laser-sheet was kept fixed during one oscillation period, and then moved to another position up till enough vertical planes were obtained to reconstruct the 3D internal wave field.

3. Data processing

The light intensity across the laser-illuminated fluorescein planes along a vertical line $I(z)$ varies as a sequence of Gaussian peaks superposed with a weak random noise. To determine the position of each maximum we calculate the cross-correlation of the experimental signal with a Gaussian $G(z, z', s_0) = \exp\left[-(z - z')^2 / 2s_0^2\right] / (\sqrt{2\pi}s_0)$. The cross-correlation of the signal with the Gaussian of fixed width s_0 is defined as $C(z') = \int I(z)G(z, z', s_0)dz$. In practice, the correlation is calculated for discrete values with the increment of 1 pixel, i.e. $C_k = \sum_{n=0}^{N-1} G_n I_{n+k}$. To reduce the computation time, the Gaussian function $G(z, z', s_0)$ is calculated once for N points, with $N = 4s_0$ to ensure that the tails of the function are sufficiently close to zero, and with the centre at $z' = 2s_0$ so that $G_n = G(n, 2s_0, s_0)$. Two methods of subpixel interpolation have been used. With the first method, three upper points at each local maximum of C_k are used to calculate the coefficients of a parabolic fit, which allow to determine the position of the maxima analytically, with subpixel accuracy. With the second method, all the nodes are used for continuous interpolation by cubic splines, and the positions of the local maxima are determined numerically with an accuracy being set at 0.05 pixel. Both methods yield essentially the same result as will be discussed below.

There exists an extensive literature on cross-correlation technique commonly used in digital PIV method (Adrian 2005, Stanislas et al 2005). In particular, practical recommendations on optimum particle size and seeding are presented in Westerweel (1997). Following Westerweel (1997), we discuss below the numerical tests elucidating the optimum choice of width s_0 of the analyzing Gaussian peak $G_n = G(n, 2s_0, s_0)$ and the effect of noise on the accuracy of subpixel interpolation.

Let us consider a test function defined as a sum of a Gaussian-type distribution and a random noise so that $I^{test}(z, z_m, s, a) = I_{max} \exp\left[-(z - z_m)^2 / 2s^2\right] + r(z, a)$, where at each point z the function $r(z, a)$ returns a random value uniformly distributed between $-a$ and a . To perform numerical tests, discrete test functions $I_i^{test} = I^{test}(i, z_m, s, a)$ are generated, where i is an integer number representing the pixel counter, and other parameters have fixed values that are representative for typical experimental data. For the tests described below we take test function $I^{test}(i, z_m, s, a)$ with known position of the maximum, z_m , prescribed at a subpixel level (say, $z_m = 101.35$), $i = 0 \dots 199$, the peak magnitude $I_{max} = 50$, and the peak width $s = 8$. The width of the analyzing Gaussian $G_n = G(n, 2s_0, s_0)$ is taken as $s_0 = 8$, i.e. equal to the width of the analyzed peak.

Further, we apply the above-described cross-correlation procedure, with a fit by quadratic parabola in the vicinity of the maximum of the discrete correlation curve C_k , to determine the position z_m of the peak maximum of I^{test} with a subpixel accuracy. The calculated position of the

maximum is denoted as z_m^c . The individual error (i.e. the error corresponding to a single realization of function $r(i, a)$ at a fixed noise level a) is defined as $z_m^c - z_m$, and measured in pixels. The statistically representative error at given a is calculated as rms value of individual errors over 20 realizations of the random function $r(i, a)$. The rms error E_{rms} as function of the normalized noise level a/I_{max} is shown in Fig. 2a, showing a clear trend, with E_{rms} increasing linearly with a/I_{max} . The slope, K , of the linear fit $E_{rms} = K(a/I_{max})$ is determined from linear regression.

The dependence of the slope K on the width of the analyzing Gaussian s_0 is shown in Fig. 2b for the parameters corresponding to the test function $I^{test}(i, z_m, s, a)$ used in figure 2a. Obviously, the optimum choice of s_0 should correspond to minimum value of K , which minimizes the overall error of the measurements. It can be seen that the slope K has a broad minimum around $s_0 = s = 8$. The range $0.5 < s_0/s < 1.5$ can be recommended as the optimum one. The dependence of K on s_0 is qualitatively similar to the one observed in Westerweel (1997) for the dependence of the typical error of cross-correlation analysis on particle size in classic PIV method.

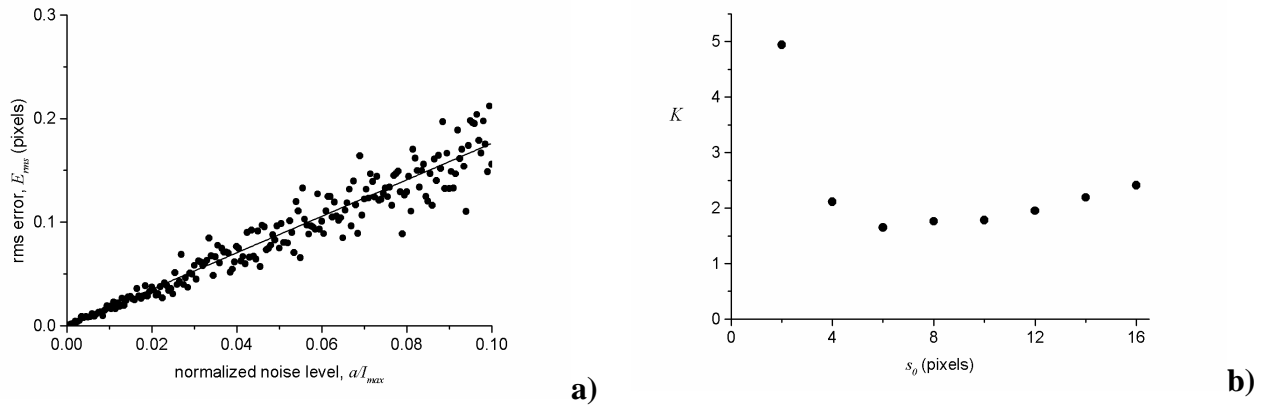


Fig. 2. Typical results obtained with the cross-correlation technique used in the present study for calculation of the position of the maximum of a Gaussian-type test function superposed with a random noise: **a)** rms error E_{rms} as function of normalized noise level a/I_{max} . The line results from regression analysis $E_{rms} = K(a/I_{max})$ with slope K . **b)** slope K of the linear dependence $E_{rms} = K(a/I_{max})$ versus the width s_0 of the analyzing Gaussian peak. Parameters of the test function are given in the text.

Let us determine the typical noise level in the real experimental data. Fig. 3a shows a typical distribution of light intensity across a fluorescein plane along a single vertical line of N pixels. The data are shown together with the best fit Gaussian curve G^{fit} resulting from application of the least-squares method. The standard error of the approximation is calculated as

$$\delta = \left(\sum_{i=1}^N (I_i - G_i^{fit})^2 / N \right)^{1/2}. \text{ It can be normalized by the magnitude of the peak of the Gaussian fit}$$

so that $\delta_{norm} = \delta/G_m$. The definition of G_m is shown in Fig. 3. For the data shown in Fig. 3a the normalized standard error of the approximation is about 0.02. The data shown in Fig. 3a have been obtained with the 8-bit camera. The analysis of the data obtained with the 12 bit camera shows the same level of the normalized error.

In the processing of real data we rarely need a spatial resolution of 1 pixel. Also, at such a high resolution (here 0.4mm) noise due to tiny scratches and impurities at the tank walls start to be relevant. For the practical implementation of the present method we use an average over M

vertical lines of pixels in horizontal direction. This procedure reduces the amount of calculations, filters out the high-frequency noise and reduces the standard error of approximation of the luminosity distribution by a Gaussian function. Typically, averaging over 10 vertical lines of pixels in horizontal direction reduces δ_{norm} by a factor of 3 to the value around 0.007. This value is nearly the same, both, for 8-bit and 12-bit cameras. In that sense the use of 12-bit camera does not offer a significant advantage as compared to a 8-bit camera. The result of averaging procedure is shown in Fig. 3b. Taking for confidence $3\delta_{norm}$ as a measure of the noise level, we note that the noise level around 0.02 in Fig. 2a corresponds to the typical error in position of the maximum of the Gaussian-type test function less than 0.05 pixel.

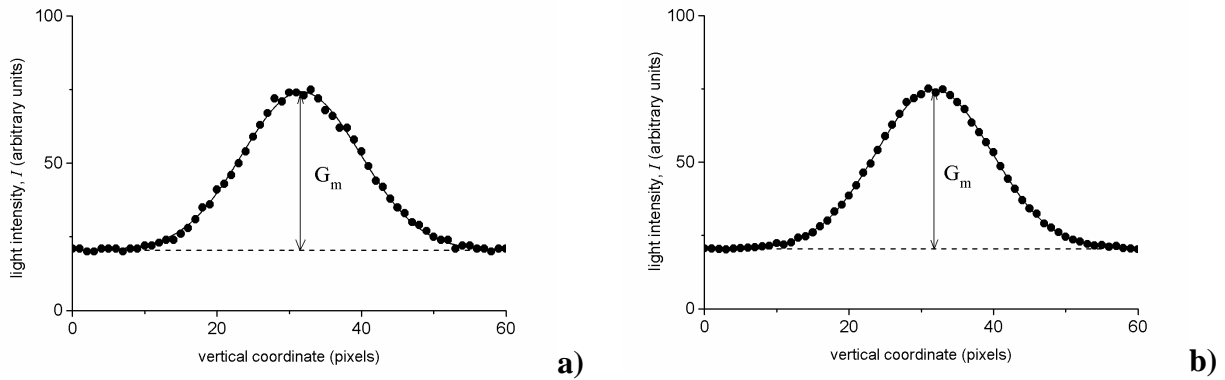


Fig. 3. Distribution of light intensity across a single fluorescein plane: dots correspond to experimental data and solid lines represent the best least squares fit by a Gaussian curve. The magnitude of the Gaussian peak with respect to the asymptotic value shown by the dashed line is denoted as G_m . The data are presented: **a)** for a single vertical line of pixels, and **b)** for an average of 10 vertical lines of pixels. The standard deviation between the experimental data and the approximations reduces by roughly a factor of 3 for the right image as compared to the left image.

4. Experimental results

In the experiments, successive images of internal wave field, generated by oscillations of the sphere and visualized by distortions of the fluorescein planes, were taken with time increment $\Delta t = 0.4$ and 0.5 s, depending on experimental conditions. The increment was sufficiently small compared to the period of oscillations so that the number of images per period was large, between 14 and 27. Accordingly, the vertical velocity could be estimated from the dye-line displacement $\Delta\zeta = \zeta(t + \Delta t) - \zeta(t)$ between two successive images, as $w(t) = \Delta\zeta / \Delta t$. Further, the velocity amplitude w_a was calculated as the period-averaged rms value of the time-series multiplied by $2^{1/2}$, similar to the procedure introduced in Sutherland and Linden (2002) and Flynn et al (2003). Finally, the non-dimensional amplitude of vertical velocity W_a is introduced using $A\omega$ as the velocity scale.

The procedure described in §3 is applied to the raw image (black and grey lines) in Fig. 4a and the result is shown as the superposed inset. In a uniformly stratified fluid, oscillations of a 3D body generate internal waves confined in a double cone, with the generatrix inclined at angle $\varphi = \arccos(\omega/N)$ to the vertical (Mowbray and Rarity 1967). A vertical cut of the cone by the plane xOz passing through the center of the sphere can be recognized in the measurement in Fig. 4a.

As it has been already mentioned, we apply two methods of subpixel interpolation (cubic spline and quadratic parabola) to determine the positions of the maxima of the cross-correlation curve. It is of interest to compare the results given by each method in the case of real image processing. A

typical result of comparison is presented in Fig. 4. In horizontal direction the data averaged over 6 vertical lines of pixels are used. The good agreement between the data obtained with the two methods of sub-pixel interpolation is evident. Note, that the maximum non-dimensional velocity amplitude for the case shown in Fig. 4b is $W = 0.35$, corresponding to dimensional velocity 1 mm/s. With the frame rate of 2.5 images per second, the maximum relative vertical dye-line displacement between two successive images in this example did not exceed 0.4mm, which corresponds to 1 pixel.

The data shown in Fig. 4b are in good agreement with the theory described in Voisin et al (2010) as a further development of the approach proposed in Voisin (2003). The reader interested in details of the theory and its cross-comparison with earlier experimental data of Flynn et al (2003), King et al (2009) and the present method is referred to Voisin et al (2010) and Ermanyuk et al (2010).

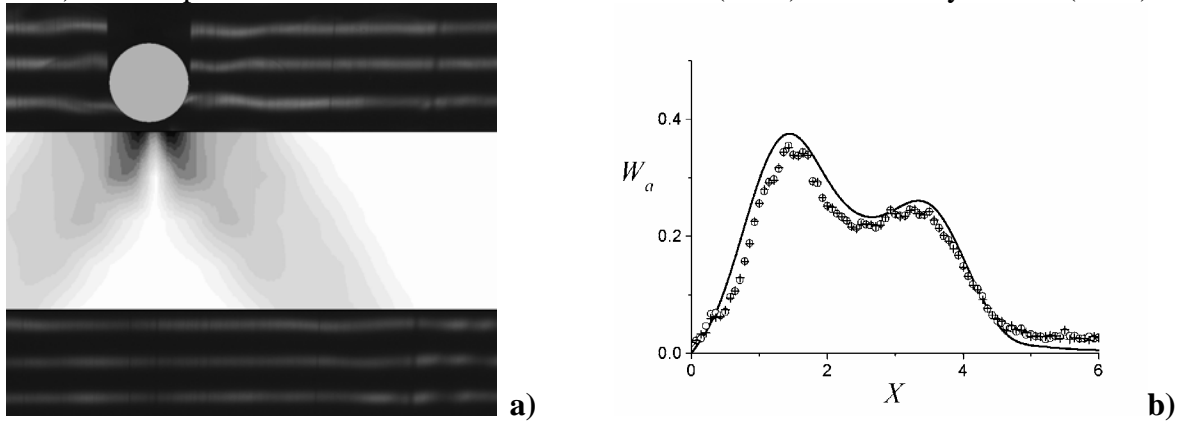


Fig. 4. a) A fragment of image shown in Fig. 1b with the superposed inset showing the result of processing, the grey levels being proportional to the amplitudes of vertical velocity, calculated from the period-averaged rms values. Data between the fluorescein layers are obtained by interpolation. **b)** Horizontal distribution of non-dimensional vertical velocity amplitude. The horizontal coordinate is non-dimensionalized by the radius of the sphere $R=3.125$ cm. The data corresponds to the fluoresceine line located at distance $2.89R$ below the center of the sphere. Solid lines show the theoretical prediction (Voisin et al 2010). Circles and crosses correspond to the subpixel interpolation of the correlation curve by cubic spline and quadratic parabola, respectively. Experimental parameters: oscillation frequency $\omega/N = 0.76$ and amplitude $A/R=0.1$.

To reconstruct the three-dimensional wave field, the wave motion was measured for a sequence of equidistant parallel planes in the y-direction (with $\Delta y = 1.6$ cm), whereas for intermediate distances spline-interpolation was used. Since the sphere oscillates horizontally, the radiation of waves is directional, with non-uniform distribution of velocity amplitude over the azimuthal angle. Such a distribution is shown in Fig. 5 representing a horizontal cross-section of the internal wave cone. Experimental data obtained for sphere of radius $R = 2.25$ cm at $A/R = 0.27$ and $\omega/N = 0.76$ are shown along with theoretical predictions (Voisin et al. 2010). Note that the maximum vertical displacement of the dye lines between two successive images for the data shown in Fig. 5 does not exceed 1 pixel, similar to the data shown in Fig. 4b. The figure reveals the characteristic bean-shaped cross-section of the velocity amplitude distribution within the wave cone. Theoretically, the velocity amplitude varies as cosine of the azimuthal angle, with maximum wave radiation along x-direction and no radiation along y-direction.

The effects at fundamental frequency ω and its multiples can be discriminated with the help of Fourier analysis similar to Zhang et al. (2007), King et al. (2009) and Thomas et al. (2009). The results of such analysis are discussed in Ermanyuk et al. (2010), where the quadrupole-type emission of the second-order internal waves is revealed and compared with dipole-type structure of the first-order waves.

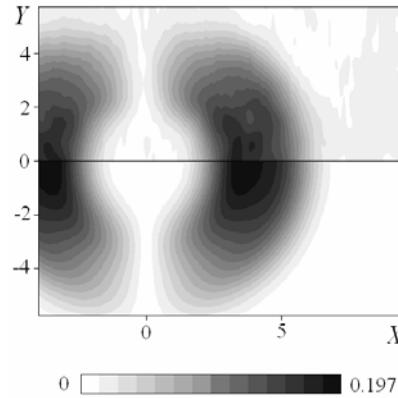


Fig. 5. Horizontal cross-section of the internal wave field at distance $Z=-5.09$ from the centre of the sphere. X – axis is oriented along the direction of oscillations, and Y – axis is directed toward the camera. All distances are non-dimensionalized by the sphere radius R . Upper (lower) part of the image shows experimental (theoretically calculated) results. The value of W_a is shown in grey levels.

5. Conclusions

This paper describes a novel technique of the 3D measurement of internal waves in a continuously stratified fluid. This method of visualization has been used before in Hopfinger et al (1991) and quantitative measurements in Flor et al. (2002) and is here adapted for high-precision low-noise automatic data processing. The method has the advantage to directly visualize the motion in a plane, to allow for the measurement of vertical velocities with high velocity gradients such as e.g. near obstacles, and gives the possibility to record also lagrangian transports.

Here it has been shown that the displacement of the dyelines can be accurately measured. Owing to molecular diffusion, the fluorescein layers have a Gaussian distribution of light intensity across each layer. The luminosity peaks are correlated with an analytically generated Gaussian function, and the correlation curve is subsequently interpolated allowing for sub-pixel resolution. The typical noise level of the data obtained with the digital cameras allows for a precise measurement of the vertical displacements of dye planes with accuracy of 0.05 pixel. Numerical tests show that the optimum width of the analyzing Gaussian closely matches the width of the luminosity peaks. The present study employs two methods of subpixel interpolation near the maxima of the cross-correlation curve. It is shown that interpolations by quadratic parabola and by cubic spline yield essentially the same results.

The translation of the laser sheet allows reconstruction of 3D internal wave fields. The present method is applied to study wave fields generated by a horizontally oscillating sphere in a uniformly stratified fluid. Good agreement is observed between experimental data and the theory described in Voisin et al. (2010). The robustness of the present method is demonstrated in application to the data corresponding to low-amplitude internal waves, when the vertical displacements of the dye planes between two successive images are below 1 pixel.

A disadvantage is that after each series of experiments the tank should be refilled. The use of a small quantity of Chlorine solution dissolved in the stratification would make the fluorescein to disappear in a number of hours

This work was performed within the French-Russian ‘Regular and Chaotic Hydrodynamics’ European Research Network. EVE acknowledges his appointment as a visiting professor at University Joseph Fourier from February-April 2009, when the experiments were performed at LEGI. EVE has been partially supported by RFBR project No. 09-01-00427 and by project 17.4 of Presidium of RAS. JBF acknowledges funding by grant FLOWing of the French Research Agency.

References

- Adrian RJ (2005) Twenty years of particle image velocimetry. *Exp Fluids* 39: 159-169
- Clark HA, Sutherland BR (2009) Schlieren measurements of internal waves in non-Boussinesq fluids. *Exp Fluids*. 47: 183-193
- Dalziel S, Hughes GO, Sutherland BR (2000) Whole-field density measurements by 'synthetic schlieren'. *Exp Fluids* 28: 322-335.
- Ermanyuk EV, Flor J-B, Voisin B (2010) Spatial structure of first and higher harmonic internal waves from a horizontally oscillating sphere. *J Fluid Mech* (submitted)
- Ermanyuk EV, Gavrilov NV (2005) Duration of transient processes in the formation of internal wave beams. *Dokl Phys* 50: 548-550
- Ermanyuk EV, Gavrilov NV (2008) On internal waves generated by large-amplitude circular and rectilinear oscillations of a circular cylinder in a uniformly stratified fluid. *J Fluid Mech* 494: 33-50
- Flor J-B, Ungarish M, Bush JWM (2002) Spin-up from rest in a stratified fluid: boundary flows. *J Fluid Mech* 472: 51-82.
- Flynn MR, Onu K, Sutherland BR (2003) Internal wave excitation by a vertically oscillating sphere. *J Fluid Mech* 494: 65-93.
- Garrett C, Kunze E (2007) Internal tide generation in deep ocean. *Annu Rev Fluid Mech* 39: 57-87
- Görtler H (1943) On an oscillatory phenomenon in fluids of a stable distribution of density. *Z Angew Math Mech* 23: 65-71
- Hazewinkel J (2010) Attractors in stratified fluids. PhD Thesis. Koninklijk Nederlands Instituut voor Zeeonderzoek (ISBN 978-90-9025020-5)
- Hopfinger EJ, Flor J-B, Chomaz J-M, Bonneton P (1991) Internal waves generated by a moving sphere and its wake in a stratified fluid. *Exp Fluids* 11: 255-261
- Ivanov AV (1989) Generation of internal waves by an oscillating source. *Izv Atmos Ocean Phys* 25: 61-64.
- King B, Zhang HP, Swinney HL (2009) Tidal flow over three-dimensional topography in a stratified fluid. *Phys Fluids* 21: 116601
- Makarov SA, Neklyudov VI, Chashechkin YuD (1990) Spatial structure of two-dimensional monochromatic internal-wave beams in an exponentially stratified liquid. *Izv Atmos Ocean Phys* 26: 548-554.
- Mercier MJ, Garnier NB, Dauxois T (2008) Reflection and diffraction of internal waves analyzed with the Hilbert transform. *Phys Fluids* 20: 086601
- Merzkirch W, Peters F (1992) Optical visualization of internal gravity waves in stratified fluid. *Opt Laser Engng* 16: 411-425
- Morozov EG (1995) Semidiurnal internal wave global field. *Deep-Sea Res I* 42: 135-148.
- Mowbray DE, Rarity BSH (1967) A theoretical and experimental investigation of the phase configuration of internal waves of small amplitude in a density stratified fluid. *J Fluid Mech* 28: 1-16
- Onu K, Flynn MR, Sutherland BR (2003) Schlieren measurement of axisymmetric internal wave amplitudes. *Exp Fluids* 35: 24-31
- Peacock T, Weidman P (2005) The effect of rotation on conical wave beams in a stratified fluid. *Exp Fluids* 39: 32-37
- Peters F. Schlieren interferometry applied to a gravity wave in a density-stratified liquid. *Exp Fluids* 3: 261-269
- Sakai S. (1990) Visualization of internal gravity wave by Moire method. *Trans Vis Soc Jpn* 10: 65-68
- Stanislas M, Okamoto K, Kahler CJ, Westerweel J (2005) Main results of the second international PIV challenge. *Exp Fluids* 39: 170-191.

- Sutherland BR, Dalziel SB, Hughes GO, Linden PF (1999) Visualization and measurement of internal waves by 'synthetic schlieren'. Part 1. Vertically oscillating cylinder. *J Fluid Mech* 390: 93-126
- Sutherland BR & Linden PF (2003) Internal wave excitation by a vertically oscillating elliptic cylinder. *Phys Fluids* 14: 721-731
- Thomas LP, Marino BM, Dalziel SB (2009) Synthetic schlieren: determination of the density gradient generated by internal waves propagating in a stratified fluid. *J Phys Conf Ser* 166: 012007
- Vlasenko V, Stashchuk N, Hutter K (2005) Baroclinic tides: Theoretical modeling and observational evidence. Cambridge University Press.
- Voisin B (2003) Limit states of internal wave beams. *J Fluid Mech* 496: 243-293
- Voisin B., Ermanyuk EV, Flor J-B (2010) Internal wave generation by oscillation of a sphere, with application to internal tides. *J Fluid Mech* (under revision)
- Westerweel J (1997) Fundamentals of digital particle image velocimetry. *Meas Sci Technol* 8: 1379-1392
- Yick KY, Stocker R., Peacock T (2007) Microscale synthetic schlieren. *Exp Fluids* 42: 41-48.
- Zhang HP, King B, Swinney HL (2007) Experimental study of internal gravity waves generated by supercritical topography. *Phys Fluids* 19: 096602